# A comprehensive slice model for continuous casting of steel

B. Šarler, B. Mavrič, T. Dobravec, R. Vertnik

A simple Lagrangean travelling slice model has been successfully used in the past to predict the relations between the process parameters and the temperature field as well as grain structure, macrosegregation assessment, optimisation of process parameters and calculation of caster regulation coefficients. The present paper aims to include also the mechanical stress and deformation model into the slice framework. The basis of all the mentioned models is the slice heat-conduction model that takes into account the complex heat extraction mechanisms in the mould, with the sprays, rolls and through the radiation. Its main advantage is very fast calculation time, amenable for use also in the caster's online control. The macroscopic model used in this study is based on the continuum mixture theory, calculating enthalpy and mixture composition as input parameters for microscopic calculations. The grain structure model is based on the cellular automata concept, replaced by a random node point automata concept. The macrosegregation model is based on the lever rule microsegregation model. The liquid phase's thermal conductivity and species diffusivity are artificially enhanced to consider the convection of the melt. The calculated thermal field is used to estimate the thermal contraction of the solid shell, which, in combination with the metallostatic pressure, drives the elastic-viscoplastic model of solid mechanics. The results of the model are used to estimate the areas susceptible to crack nucleation using several hot-tearing and damage models. The solution procedure of all the models is based on the meshless local radial basis function collocation method on the macroscopic scale and the point automata concept on the grain structure scale. A sensitivity study on the recently introduced standard continuous casting geometry is performed as well as on the realistic conditions in Štore-Steel billet caster. Possible additional refinements of the model are discussed.

**KEYWORDS:** CONTINUOUS CASTING OF STEEL, SLICE MODEL, TEMPERATURE, GRAIN STRUCTURE, MACROSEGREGATION, STRESS AND STRAIN

## INTRODUCTION

Computational modelling and simulation of the continuous casting process [1] represent essential contemporary information about the process [2]. The slice model of the thermal field is neglecting diffusion processes in the direction of the casting and convection processes perpendicular to the casting direction. Such a model, coupled with the realistic material properties of the steel has been recognised by the technologists as one of the most powerful tools for establishing the relations between the process parameters of the caster and the thermal field, optimal adjustment of casting parameters, and estimating the changes in the design of the caster [3]. Due to its fast computational time, the slice model can be used in on-line mode and for automation of the caster [4]. It is the purpose of the present paper to show how the thermal slice model can be accompanied with a simple grain structure, macrosegregation and mechanical

Božidar Šarler
University of Ljubljana and Institute of Metals and Technology, Slovenia

Boštjan Mavrič
Institute of Metals and Technology and University of Ljubljana, Slovenia

Tadej Dobravec
University of Ljubljana, Slovenia

Robert Vertnik
University of Ljubljana and Štore Steel, Slovenia

models, which additionally enhance the functionality of the thermal model and give fast and at least qualitative insight into CET position, composition inhomogeneities, stresses and strains of the strand. The model can also be used for piloting more comprehensive multiphysics simulations [5] that can be performed on high-performance systems only.

## THERMAL MODEL

The thermal model considers the heat diffusion in steel undergoing phase change

$$\frac{\partial(\rho h)}{\partial t} = \nabla \cdot (k \nabla T), \qquad (1)$$

where ρ, h, k, and T stand for the density, the specific enthalpy, the heat conductivity, and the temperature, respectively. The equations that follow are, because of the space constraints, shown for a binary system, however, a linearised multicomponent system is actually numerically implemented and solved. The mixture formulation [6] is used to describe a system containing the solid and the liquid phase. The constant density is assumed. The mixture enthalpy is given as

$$h = f_s h_s + (1 - f_s) h_l , \qquad (2)$$

where $f_s$ is the solid fraction and the subscripts s and l represent the solid and liquid phase, respectively. In the case of constant specific heat in each phase, the enthalpies in the solid and in the liquid phase are determined as

$$h_s = h_{ref} + c_{ps}(T - T_{ref}), \quad h_l = h_{ref} + c_s(T_{sol} - T_{ref}) + h_m + c_l(T - T_{sol}) , \qquad (3)$$

where $h_{ref}$, $T_{ref}$, $c_p$, $T_{sol}$ , and $h_m$ stand for the reference enthalpy, the reference temperature, the specific heat, the solidus temperature, and the latent heat of melting, respectively. The enthalpy as a function of temperature in a binary alloy is shown in Fig. 1.

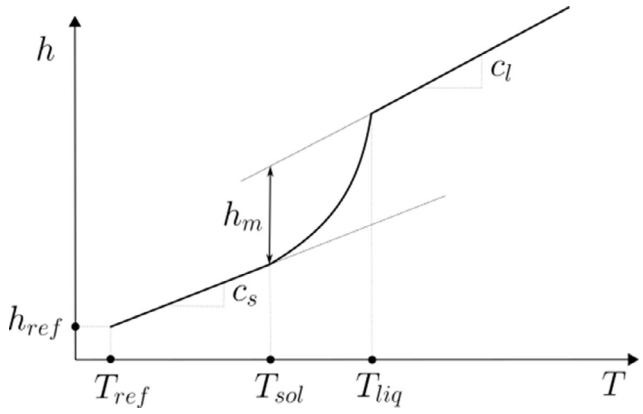


**Fig.1** - The enthalpy as a function of temperature in a binary alloy.

The mixture thermal conductivity is given as

$$k = f_s k_s + (1 - f_s) k_l . \qquad (4)$$

The lever rule is used as supplementary micro-segregation relation

$$C = f_s C_s + (1 - f_s) C_l , \quad C_s = k_p C_l , \qquad (5)$$

where C and $k_p$ stand for the concentration and the partition coefficient, respectively. The linearised phase diagram is used to obtain the temperature dependence on the concentration in the liquid phase

$$T = T_m + m_l C_l , \qquad (6)$$

where $T_m$ and $m_l$ stand for the melting temperature of the solvent and the liquidus slope, respectively.

## MECHANICAL MODEL

The mechanical model is stated in small-deformation approximation and considers additive decomposition of strain into elastic, thermal and viscoplastic parts [7]. The thermal part is determined by

$$\varepsilon^t = I\int_{T_{ref}}^{T} \alpha(T)dT, \qquad (7)$$

where α(T) is the temperature-dependent coefficient of thermal expansion. The viscoplastic part is given by the Garafalo law [8]

$$\dot{\varepsilon}^{vp} = A_0 \exp(-q/T)\left(\frac{\sigma_e}{\sigma_0}\right)^n. \qquad (8)$$

The parameters $A_0$, q, n and $\sigma_0$ are determined from the least-squares fit of the high-temperature flow-stress data obtained from a suitable steel material properties software or measurements. The influence of the metallostatic pressure is introduced through an additional body force term given by $f_b=p_m\nabla f_s$, where $p_m$ is the metallostatic pressure at the centre of the slice and fs is the solid fraction. The resulting equilibrium equation for the displacement field is

$$-p_m\nabla f_s = G\nabla^2\mathbf{u} + (G+\lambda)\nabla\nabla\cdot\mathbf{u} + \nabla\lambda\nabla\cdot\mathbf{u} + \nabla G\left(\nabla\mathbf{u} + (\nabla\mathbf{u})^T\right) - \nabla\cdot\left(G\varepsilon^{vp}\right) - \nabla\cdot\left((3\lambda+2G)\varepsilon^t\right). \qquad (9)$$

The boundary of the domain is assumed to be traction free everywhere, and the influence of the mechanical contact with the mould and rolls is neglected in the present model.

## GRAIN STRUCTURE MODEL

The grain structure model takes into account the heterogeneous nucleation and the grain growth [8]. The normal distribution is used to describe the change of nucleation density n due to the shift in the undercooling ΔT

$$\frac{dn}{d\Delta T} = \frac{n_{max}}{\sqrt{2\pi}\Delta T_\sigma}\exp\left[-\frac{1}{2}\left(\frac{\Delta T - \Delta T_\mu}{\Delta T_\sigma}\right)^2\right], \qquad (10)$$

where $n_{max}$, $\Delta T_\sigma$, and $\Delta T_\mu$ stand for the maximum nucleation density, the scale, and the mean of the undercooling, espectively. The LGK [10,11] model is applied to evaluate grain growth velocity at given ΔT. The model yields a system of two non-linear equations for two unknowns: the grain growth velocity v* and the dendrite's tip radius $R_{tip}$. The model considers thermal, solutal, and curvature effects as the Ivantsov solution is used for the temperature and concentration fields in the liquid phase. The minimum wavelength from the stability analysis for the planar front is used to estimate the tip radius. At low undercooling, the thermal and curvature effects can be neglected [12], which yields the following simple approximate expression for the growth velocity

$$v^* = \frac{D_l}{5.51\pi^2(-m_l(1-k_p)C_0)^{1.5}\Gamma_{sl}}\Delta T^{2.5}, \qquad (11)$$

where $D_l$, $C_0$, and $\Gamma_{sl}$ stand for the solute diffusivity in the liquid phase, initial concentration, and the GibbsThomson coefficient, respectively.

## MACROSEGREGATION MODEL

The macrosegregation model considers the diffusion of solute. The one-sided approximation is assumed where only the diffusion of solute in the liquid phase is considered

$$\frac{\partial(\rho C)}{\partial t} = \nabla\cdot(\rho f_l D_l \nabla C_l). \qquad (12)$$

Eqs. (1) and (12) are solved simultaneously as T, $C_l$, and fs at given C and h are calculated by solving a system of three non-linear equations given by combining relations from Eqs. (2), (3), (5), and (6). The influence of the turbulent fluid flow on the macrosegregation is taken into account through the artificially increased liquid diffusivity [13] by factor 10, i.e., $D_l \rightarrow 10D_l$ in Eq. (9).

## NUMERICAL SOLUTION

### SOLUTION OF THERMAL AND MACROSEGREGATION MODEL

The coupled thermal and macrosegregation models are solved on the regular node distribution with the spacing $h_{thermal}$ by using forward Euler scheme for temporal and local radial basis function collocation method (LRBFCM) [13] with five computational nodes in each local sub-domain for spatial discretisation. In the LRBFCM, multiquadrics (MQs) are used as radial basis functions, and the interpolation problem is augmented with monomials up to the first order. The shape

parameter of an MQ in each local domain is chosen according to the targeted condition number $10^{20}$ of the interpolation matrix. The time step in the forward Euler scheme is

$$\Delta t_{thermal} = 0.2\frac{h_{thermal}^2}{\max(D_{Ts}, D_{Tl})}, \quad D_T = \frac{k}{\rho c_p}, \tag{13}$$

where $D_T$ is the thermal diffusivity.

## POINT AUTOMATA METHOD

The Point automata (PA) method [15] is used to simulate nucleation and grain growth where ΔT as a function of time is given by the thermal model. In the PA method, the computational points are randomly distributed in the computational domain. The neighbourhood of each point is defined by the points which lie inside the circle with radius $R_{PA}=1.5h_{PA}$, where $h_{PA}$ is the characteristic spacing between the two neighbouring points. Each point has a defined state which is either solid or liquid. A solid point has additionally defined grain number and orientation angle ϑ. All the points in the computational domain are checked with the time step $\Delta t_{PA}=\Delta t_{thermal}/M$, where $\Delta t_{thermal}$ and M stand for the time interval between two sequential temperature fields obtained from the thermal model and the number of divisions of $\Delta t_{thermal}$, respectively. In the nucleation procedure, a liquid point changes its state to solid if

$$r < V_{PA} \int_{\Delta T}^{\Delta T+\delta(\Delta T)} \frac{dn}{d(\Delta T')} d(\Delta T'), \tag{14}$$

where r is a random number in the range [0,1), $V_{PA}$ is the volume represented by a point, and δ(ΔT) stands for the change of ΔT during one time step while the change of the nucleation density due to the change of the undercooling is given by Eq. (10). At the same time, random grain number and random orientation angle ϑ are assigned to the newly nucleated point.

In the grain growth procedure is the distance for each solid point, which has at least one liquid neighbour, calculated as

$$l(t) = \int_{t_0}^{t} v^*(\Delta T)dt, \tag{15}$$

where $t_0$ is the time at which the nucleation occurred, and the growth velocity is given by Eq. (11). The solid point captures its liquid neighbour if

$$d \le l(t)\left[\frac{1+\alpha}{2} - \frac{1-\alpha}{2}\cos\left(4(\theta-\phi)\right)\right], \quad \phi = \arctan(d_y/d_x), \quad d = \sqrt{d_x^2+d_y^2}, \tag{16}$$

where d is the distance between the solid and liquid point and α stands for the ratio between the minimum and the maximum distance in the envelope. When a liquid point is captured, its grain number and orientation angle are set according to the values of the solid capturer. The PA growth algorithm is schematically shown in Fig.

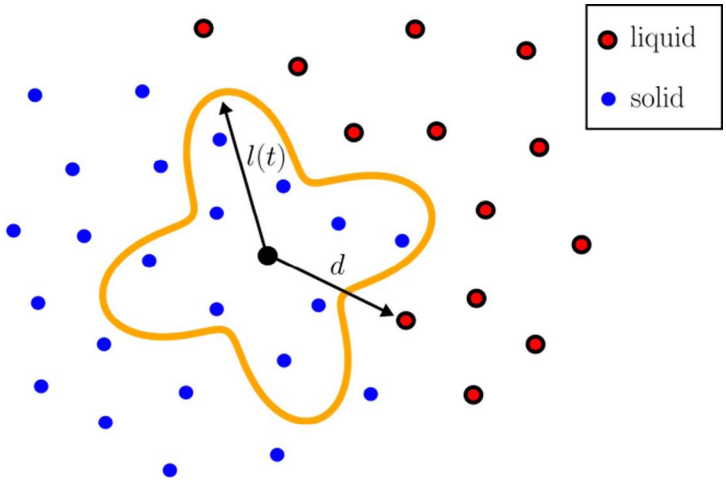


**Fig.2** - A scheme of the PA algorithm for the simulation of grain growth.

## MECHANICAL MODEL

The system of equations defining the thermomechanical model from Eqs. (8) and (9) is discretised with implicit Euler method in time and with LRBFCM in space. The LRBFCM uses polyharmonic splines with second-order augmentation monomials and 18 points in local subdomains. The coupling between models is one-way, the information about the temperature field is used to drive the thermomechanical model. A step of the thermal model is performed, and the obtained temperature field is used to drive the thermomechanical model for the duration of the time step. The time-stepping of the thermomechanical model is adaptive, based on the convergence rate of the non-linear solver.

The thermomechanical model uses an adaptive node arrangement, which tracks the solidification interface through the computational domain with nodes concentrated in the mushy zone. The node spacing varies from 0.5 mm in the mushy zone to 1 mm in the solid shell and 5 mm in the liquid part of the computational domain.

## TEST PROBLEM DEFINITION AND NUMERICAL RESULTS THERMAL AND MACROSEGREGATION MODEL

In the study, a simple test case initially proposed in [13] is considered to demonstrate all the elements of the developed comprehensive slice model. A two-dimensional square computational domain with the side length L=0.14 m is considered. The domain is discretised by regular node distribution with spacing $h_{thermal}$=1 mm. The square represents a slice that lies in the xy-plane and travels in the z-direction with the constant casting velocity $v_{cast}$=1.75 m/min. The z coordinate of the slice as a function of time is in that case simply given as

$$z(t) = z_0 + v_{cast}(t - t_0), \qquad (17)$$

where $z_0$ and $t_0$ are the initial axial coordinate and the initial time, respectively, both set to zero in the study.

Therefore, the time integration of governing equations in the xy-plane is also moving of the slice in the zdirection.

In the thermal model, the Robin boundary conditions are applied for the temperature. They take into account cooling in the mould (z<0.8 m) and in the spray section (z≥0.8 m)

$$-k\nabla T \cdot \mathbf{n} = h_{mold}(T - T_{cool}), \quad -k\nabla T \cdot \mathbf{n} = h_{spray}(T - T_{cool}) \qquad (18)$$

where n is the normal to boundary of computational domain, $h_{mold}$ and $h_{spray}$ are the heat transfer coefficients in the mould and spray region, respectively, and $T_{cool}$ is the cooling temperature. The parameters of the boundary conditions are set to $h_{mold}$=2000 W/(m²K), $hs_{pray}$=800 W/(m²K), and $T_{cool}$=303 K. In the macro-segregation model, zero flux Neumann boundary conditions are used for the concentration.

The solidification in Fe-0.8wt.%C steel is considered in the study. The relevant physical and phase diagram properties of the alloy are given in Table 1. The initial temperature in the domain is set 20 K above the liquidus temperature at the initial concentration $C_0$=0.8wt.%C.

**Tab.1** -Physical and phase diagram properties of Fe-0.8wt.%C.

| **Physical and phase diagram properties of Fe-0.8wt.%C** | **Value** | |
|---|---|---|
| Density | $\rho$ [kg/m³] | 6990.0 |
| Specific heat (liquid) | $c_{pl}$ [J/(kgK)] | 1395.8 |
| Specific heat (solid) | $c_{ps}$ [J/(kgK)] | 824.9 |
| Thermal conductivity (liquid) | $k_l$ [W/(mK)] | 39.3 |
| Thermal conductivity (solid) | $k_s$ [W/(mK)] | 25.0 |
| Latent heat of melting | $L_m$ [J/kg] | $2.71 \times 10^5$ |
| Solute diffusivity | $D_l$ [m²/s] | $1.36 \times 10^{-9}$ |
| Melting temperature of Fe | $T_m$ [K] | 1835 |
| Eutectic temperature | $T_{eut}$ [K] | 1420 |
| Eutectic concentration | $C_{eut}$ [wt.%] | 4.3 |
| Partition coefficient | $k_p$ [-] | 0.521 |
| Gibbs-Thomson coefficient | $\Gamma_{sl}$ [Km] | $3 \times 10^{-7}$ |

The temperature in the middle of the computational domain and at the surface (middle of west side) as a function of z coordinate is shown on the left in Fig. 3. Naturally, a large difference between the temperature profiles is observed. At z=0.8 m, a jump of the temperature at the surface is observed due to the change of the heat transfer coefficient. The concentration in the solid phase by the middle cross section in the solidified strand is shown on the right in Fig. 3. Large negative segregation is observed at the surface due to temperature drop because of high cooling rates in the mould. Small positive peaks are observed at |x|≈6.8 cm due to depleted solid near the surface and high cooling rates. The negative peaks at |x|≈5.5 cm and the positive central segregation are the consequence of the advection of solute to the centre due to the intensive turbulent fluid flow, simply modelled by the enhanced thermal conductivity and diffusivity of the liquid phase.

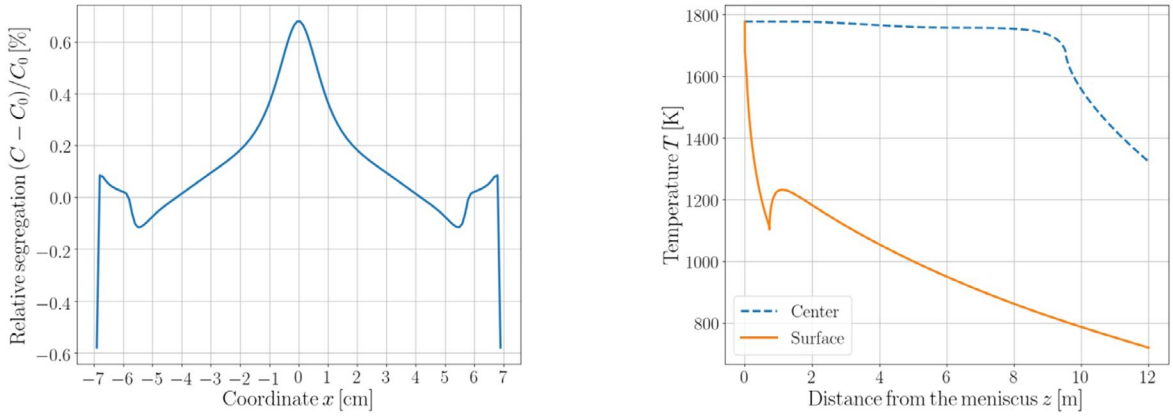


**Fig.3** - (left) Temperature in the middle and at the surface (middle of west side) of the slice as a function of z coordinate. (right) The concentration in the solid phase by the middle cross-section in the solidified strand.

## GRAIN STRUCTURE MODEL

In the PA model, the computational domain is discretised by randomly distributed points with the mean spacing $h_{PA}$=0.1 mm. The number of divisions of the time step from the thermal model is set to M=100. Two maximal nucleation densities are used, one at the boundary and one in the bulk of the computational domain. The nucleation densities are generally defined in 3-D. Following relations have to be used to obtain appropriate values in 2-D [9]

(19)

$$n^{3D}_{max,surf} = \frac{\pi}{4}(n^{2D}_{max,surf})^2, \quad n^{3D}_{max,bulk} = \sqrt{\frac{\pi}{6}}(n^{2D}_{max,bulk})^{3/2}.$$

max surf max surf max bulk max bulk n n n n (19)

The used parameters of the PA model are shown in Table 2.

**Tab.2** - Parameters of the PA model.

| **Parameters of the PA model** | | |
|---|---|---|
| Max. nucleation density (surface) | $n_{max,surf}$ [1/m²] | 1x10¹⁰ |
| Max. nucleation density (bulk) | $n_{max,bulk}$ [1/m³] | 1x10⁸ |
| Mean undercooling (surface) | $\Delta T_{\mu,surf}$ [K] | 0.1 |
| Mean undercooling (bulk) | $\Delta T_{\mu,bulk}$ [K] | 0.1 |
| Scale undercooling (surface) | $\Delta T_{\sigma,surf}$ [K] | 0.001 |
| Scale undercooling (bulk) | $\Delta T_{\sigma,bulk}$ [K] | 0.001 |
| The envelope ratio | α [-] | 0.25 |

The final microstructure is shown in Fig. 4. Due to high nucleation density, an equiaxed dendritic zone with many differently oriented grains is observed at the surface. Due to growth in a temperature gradient, columnar dendritic growth is observed near the surface. It is evident that the grains with orientation parallel to the temperature gradient are more privileged. In the undercooled liquid ahead of the growing columnar grains, nucleation becomes more and more dominant as the columnar front moves towards the centre. At a certain point, the columnar dendrites are totally blocked from the newly nucleated grains, which yields large equiaxed zone in the middle of the domain.

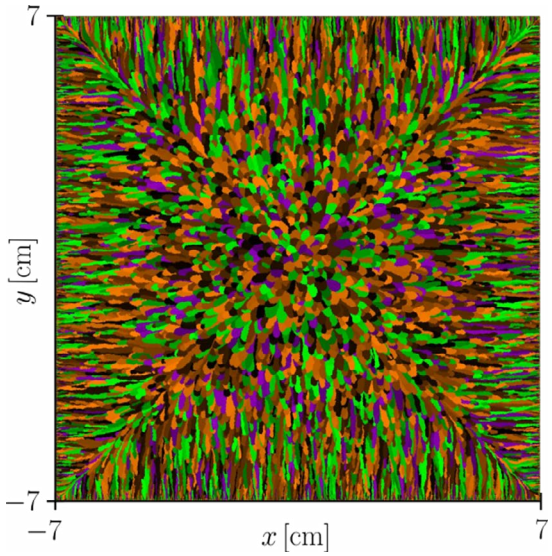


**Fig.4** - Final microstructure in the solidified slice.

## MECHANICAL MODEL

The parameters of the mechanical model are chosen such that they correspond to high-strength steel and are collected in Table 3.

**Tab.3** - Parameters of the mechanical model

| Parameter | | |
|---|---|---|
| Young's modulus | E [Pa] | $270 \times 10^9 f_s$ |
| Poisson's ratio | ν[-] | 0.3 |
| Reference stress | $\sigma_0$ [Pa] | $5 \times 10^8$ |
| Stress exponent | n[-] | 6 |
| Reference strain rate | $A_{0f}$[1/s] | 0.34 |
| Activation energy | q [K] | $6.340 \times 10^3$ |
| Thermal expansion coefficient | α [-] | 0.707 |

The results in Fig. 5 show the equivalent stress, components of stress tensor and solid fraction at the exit of the mould cooling area. The Fig. 6 shows the same at the end of the liquid root, where the entire billet has solidified. We can notice that the plastic deformations start to accumulate in the corners of the billet, but in later stages, the plastic deformation mostly accumulates along the sides of the billet, which are in tension. From the plots of the stress tensor components, we also notice that except for the corners, the material is in compression at the start of the casting process.

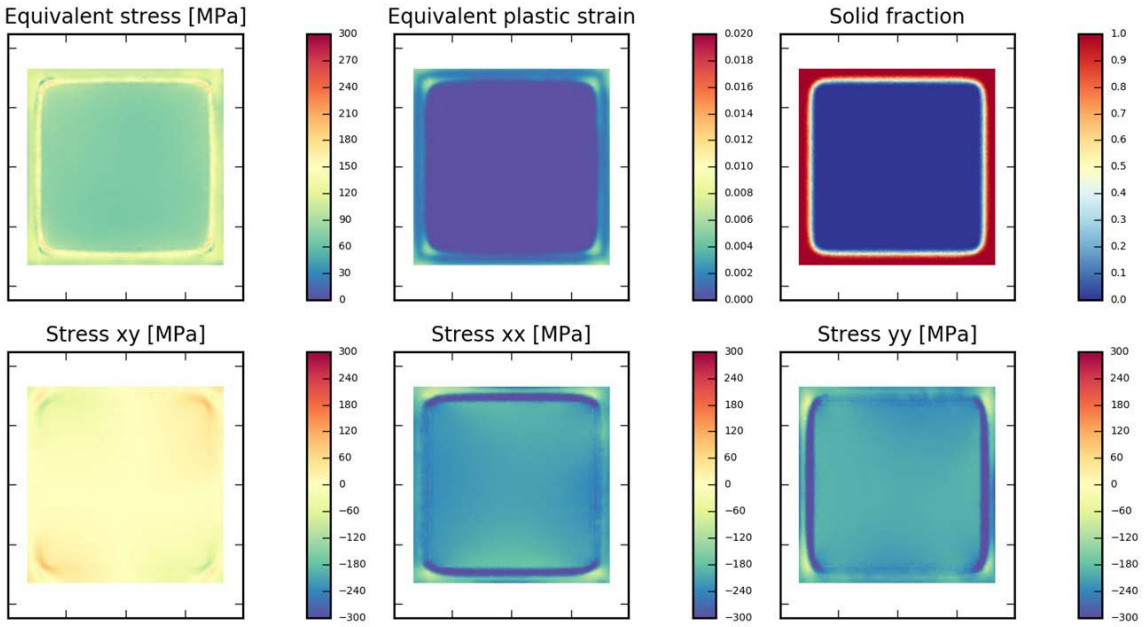


**Fig.5** -The results of the mechanical model at the exit from the mould cooling area.

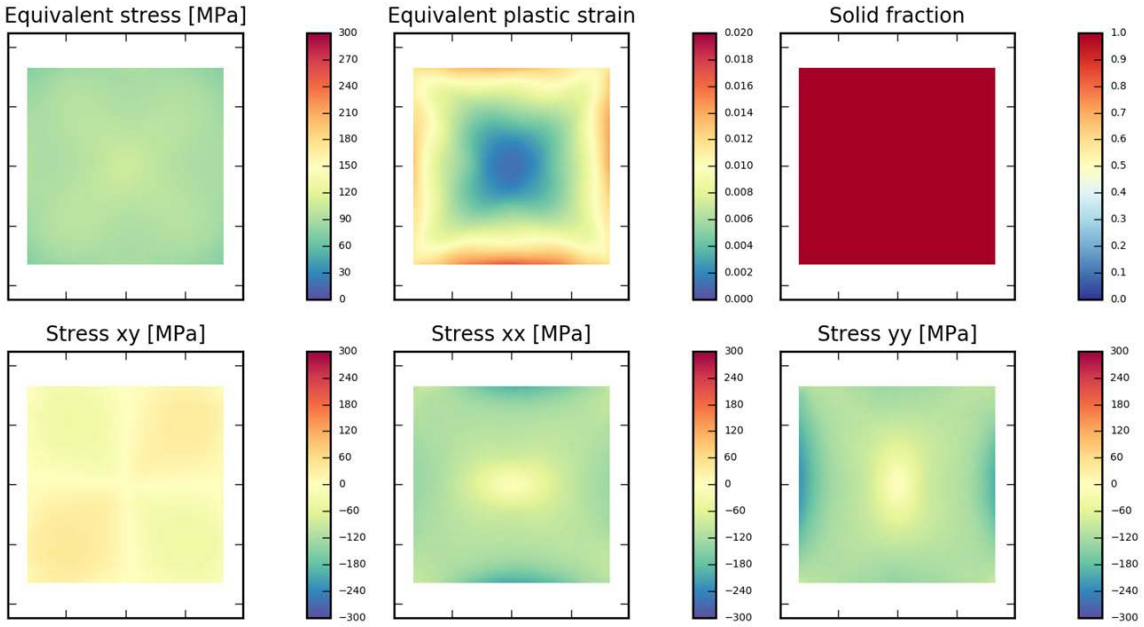


**Fig.6** -The results of the mechanical model at the end of solidification.

## CONCLUSIONS

We have in the present paper joined the majority of the important physical phenomena that a simple slice model could qualitatively describe. We have demonstrated the capabilities of the model based on a simple test case. During the conference, we will show the capabilities of the model based on realistic simulations for a billet, round and slab caster. We will also demonstrate the validation of the comprehensive slice model, based
on temperature measurements of the surface, wedge method for the thickness of the strand, Baumann prints for grain structure and laser shape measurements of the deformation. The developed model is productively used in Štore-Steel company billet caster for all the possible purposes, defined in the introduction. It also forms a part of the comprehensive through-process modelling [16, 17] of the steel plant, based on the chain of coupled physics-based and artificial intelligence models.

## ACKNOWLEDGEMENT

The present work was funded by the Slovenian Research Agency (ARRS) in the framework of applied research project L2-9246 Multiphysics and Multiscale Numerical Modelling for Competitive Continuous Casting, program P2-0162 Transient two-phase flows and Štore-Steel company (www.store-steel.si).

## REFERENCES

[1] Thomas BG. Review on modeling and simulation of continuous casting. Steel Research International. 2017; 89: 1700312. https://doi:10.1002/srin.201700312
[2] Branca TA, Fornai B, Colla V, Murri MM, Streppa E, Schröder AJ. The challange of digitalization in steel industry. Metals. 2020; 288: 1-23.
[3] Šarler B, Vertnik R, Šaletić S, Manojlović G, Cesar J. Application of continuous casting simulation at Štore Steel. BHM: Berg- und Hüttenmänische Monatshefte. 2005; 150: 300-306.
[4] Šarler B, Vertnik R, Guštin A, Vušanović I, Senčič B. Application of continuous casting simulation at Štore Steel II. BHM: Berg- und Hüttenmänische Monatshefte. 2014; 159: 99-107.
[5] Vertnik R, Mramor K, Šarler B. Solution of three-dimensional temperature and turbulent velocity field in continuously cast steel billets with electromagnetic stirring by a meshless method. Engineering Analysis with Boundary Elements. 2019; 104: 347-363.
[6] Bennon WD, Incropera FP. A continuum model for momentum, heat and species transport in binary solid-liquid phase change systems—I. Model formulation. Int J Heat Mass Tran. 1987; 30: 2161–2170.
[7] Mavrič B, Dobravec T, Vertnik R, Šarler B. A meshless thermomechanical travelling-slice model of continuous casting of steel. IOP conference series. Materials science and engineering. 2020, 861: 1-8
[8] Koric S.,Thomas BG. Thermo-mechanical models of steel solidification based on two elastic visco-plastic constitutive laws, Journal of Materials Processing Technology. 2008; 197: 408–418.
[9] Rappaz M, Gandin Ch.-A. Probabilistic modelling of microstructure formation in solidification processes, Acta Metallurgica et Materialia. 1993; 41: 345–360.
[10] Lipton J, Glicksman ME, Kurz W. Dendritic growth into undercooled alloy metals. Materials Science and Engineering. 1984; 65: 57–63.
[11] Lipton J, Glicksman ME, Kurz W. Equiaxed dendrite growth in alloys at small supercooling. Metall and Mat Trans A. 1987; 18: 341–345.
[12] Dantzig JA, Rappaz M. Solidification, 2nd Edition, EPFL Press, Lausanne, Switzerland; 2016.
[13] Vušanović I, Vertnik R, Šarler B. A simple slice model for prediction of macrosegregation in continuously cast billets. IOP Conf. Ser.: Mater. Sci. Eng. 2012; 27: 012056.
[14] Šarler B, Vertnik R. Meshfree explicit local radial basis function collocation method for diffusion problems. Comput Math Appl. 2006; 51: 1269–1282.
[15] Lorbiecka A, Vertnik R, Gjerkeš H, Manojlovič G, Senčič B, Cesar J, Šarler B. Numerical Modeling of Grain Structure in Continuous Casting of Steel. Comput Mater Contin. 2008; 8: 195–208.
[16] Hanoglu U, Šarler B, Multi-pass hot-rolling simulation using a meshless method. Computers & Structures. 2018; 194: 1-14.
[17] Kovačič M, Stopar K, Vertnik R, Šarler B. Comprehensive electric arc furnace electric energy consumption modeling: a pilot study. Energies. 2019; 12: 1-13.